RSC Advances

PAPER

Cite this: *RSC Adv.*, 2016, **6**, 26111

Zinc oxide quantum dots: multifunctional candidates for arresting C2C12 cancer cells and their role towards caspase 3 and 7 genes†

Rizwan Wahab,*[ab] Farheen Khan,[c] You bing Yang,[d] I. H. Hwang,[e] Hyung-Shik Shin,[f] Javed Ahmad,[ab] Sourabh Dwivedi,[g] Shams T. Khan,[ab] Maqsood A. Siddiqui,[ab] Quaiser Saquib,[ab] Javed Musarrat,[gh] Abdulaziz A. Al-Khedhairy,[a] Yogendra Kumar Mishra[i] and Bahy A. Ali[bj]

Received 2nd December 2015
Accepted 22nd February 2016

DOI: 10.1039/c5ra25668b

www.rsc.org/advances

Recently, nanoscale (<100 nm) inorganic materials, especially spherical shaped zinc oxide quantum dots (ZnO-QDs), have received a lot of attention from the broad community because of their potential utilization in various technologies. Due to their large surface to volume (*S*/*V*) ratios and extremely high reactivities, they can easily penetrate in various biological identities, such as cells and proteins, and therefore can sense, diagnose and cure different biological systems. The present study describes the facile synthesis of crystalline ZnO-QDs *via* a solution process. In addition, C2C12 myoblast cancer cells have been treated with different doses of ZnO-QDs at different incubation times (24, 48, 72 and 96 h). The rate of inhibition of cells was observed using an MTT assay, whereas the morphology of the cells was observed by confocal microscopy (CLSM). The MTT and CLSM investigations confirmed that with an increase in the incubation time, the population density of cancer cells was decreased when treated with ZnO-QDs. The dose dependent apoptosis correlated with intracellular production of reactive oxygen species (ROS) from C2C12 cancer cells was also measured in presence of ZnO-QDs. Moreover, the effect/apoptosis of these QDs was also checked in the presence of candidate genes such as caspase 3/7 with GAPDH. Reverse transcription polymerase chain reaction (RT-PCR) analysis demonstrates the up-regulation of caspase 3/7 genes in cells subsequently treated with ZnO-QDs at low and high concentrations.

Introduction

Cancer is currently a very major issue in the society because of the many deaths linked to this disease with the biomedical society still looking for appropriate alternative therapies, which can kill cancer cells but at the same time it must be biocompatible so that normal and healthy cells remain unaffected. Recent developments in nanotechnology have provided new platforms of different types of nanostructures, which can be effectively used in biomedical engineering for various treatments. Owing to their *S*/*V* ratio in the nanoscale region, these nanostructures exhibit extraordinary physical and chemical features, which enable them as potential building blocks for several multifunctional applications in different disciplines and particularly in the biomedical field. For example, very small nanostructures (~1–100 nm) can be effectively utilized to identify and cure diverse categories of cancers.[1] Different nanostructures find potential roles for the detection of DNA, intracellular labelling, drug delivery, and blocking viral entry into the cells, cancer targeting and imaging.[2–11] Moreover, they are heavily utilized in cell and molecular biology as markers and probes and for tissue engineering, clinical bio-analytical diagnostics and therapeutics.[11,12] In particular, the nanostructures of metal oxides are significantly used by industries for making several products in the market for day-to-day life such as cosmetics, catalysts, fillers and drug carriers.[13] Among various metal oxides, zinc oxide nanostructures have drawn special attention from materials scientists due to their biocompatible nature, low cost, and ease of processing and

[a]*Zoology Department, College of Science, King Saud University, Riyadh 11451, Saudi Arabia. E-mail: rwahab05@gmail.com; rwahab@ksu.edu.sa; Tel: +966-536023284*

[b]*Al-Jeraisy, Chair for DNA Research, Department of Zoology, College of Science, King Saud University, Riyadh 11451, Saudi Arabia*

[c]*Department of Chemistry, Aligarh Muslim University, Aligarh 202002, UP, India*

[d]*Animal Science & Technology College, Henan University of Science and Technology, China*

[e]*Department of Animal Resources and Biotechnology, Chonbuk National University, Jeonju 561-756, Republic of Korea*

[f]*Energy Materials & Surface Science Laboratory, Solar Energy Research Center, School of Chemical Engineering, Chonbuk National University, Jeonju 561-756, Republic of Korea*

[g]*Dept. of Ag. Microbiology, AMU, Aligarh, India*

[h]*Baba Gulam Shah Badshah University, Rajouri, J&K, India*

[i]*Institute for Materials Science, Functional Nanomaterials University of Kiel, Kaiser Str. 2, 24143 Kiel, Germany*

[j]*Department of Nucleic Acids Research, Genetic Engineering and Biotechnology Research Institute, City for Scientific Research and Technological Applications, Alexandria, Egypt*

† Electronic supplementary information (ESI) available. See DOI: 10.1039/c5ra25668b

have already shown potential applications in various fields such as sunscreens, photocatalysis, cosmetic products, and optoelectronic devices.[14–16] In this regard, ZnO nanostructures, which have very small size (diameter < 10 nm), are known as quantum dots (QDs) and are particularly important because of their very high *S*/*V* ratio and therefore high reactivity. Being from direct semiconductor family and possessing a bandgap (~3.37 eV) similar to that of TiO_2 (~3.23 eV), ZnO-QDs include extraordinary fluorescent features helpful for identification or treatment. Because of their very small diameter (<10 nm), these ZnO-QDs can easily penetrate cells, viruses, proteins and other biological identities. ZnO-QDs are also superior to conventional organic-based nanomaterials because of their high durability, chemical stability, ease of synthesis, low cytotoxicity, increased selectivity, and heat resistant.[17] In addition, ZnO nanostructures offer the unique feature of strong photosensitizing (PS) behaviour, which can be very useful in various photodynamic and skin care therapies because of their ultra-small quantum size.[18–20] The QDs are constrained on the upper part of the stratum corneum, which provides effective optical response affected *via* UV-light.[21] These QDs exhibit the ability to reduce the growth of cancer cells due to their cytotoxic nature. In this context, muscle cells provide an excellent model to evaluate the functionality of candidate genes in the caspase series, which are the family of cysteine aspartate-specific genes with 14 members. Caspases play an important role in cell inflammation or apoptosis and are categorized into three different classes, which depend on their character.[22] In the process of apoptosis, caspases are further subdivided into initiator caspases (8, 9, 10 and 11) and effector caspases (3, 6 and 7), which are dependent on the location of the cell death pathway.[22]

The effector caspases (3, 6 and 7) are responsible for interruption in cells after the initiation of apoptosis. They catalyse the whole cells and damage the cellular proteins, which is a major reason of cell death and are accountable for disordering the cell as the apoptosis process initiates. Caspases also target caspase-activated DNase.[23,24]

Herein, we report the very promising activity of highly crystalline ZnO-QDs against myoblast C2C12 cancer cells. The effective inhibition of the growth of cancer cells with ZnO-QDs in a dose dependent manner has been analyzed against C2C12 cells for the first time. The ZnO-QDs used were synthesized *via* a soft chemical non-aqueous solution process, which facilitates a simple and cost effective synthesis of highly crystalline ZnO-QDs in large amounts. The effect/apoptosis using ZnO-QDs also validated their toxic behavior against cancer cells in presence of candidate genes such as caspase 3 and caspase 7 with GAPDH genes. The process of ZnO-QDs interaction with cancer cells is also discussed as an illustration.

Materials and methods

Experimental

Synthesis of ZnO-QDs. For the formation of ZnO-QDs, the precursor zinc acetate dihydrate ($Zn(AC)_2 \cdot 2H_2O$, 0.3 M) and *n*-propyl amine (CH_3–$(CH_2)_2$–NH_2) (20 mL) were mixed in 100 mL of methanol and stirred for 30 min. The chemicals related to the formation of the QDs, such as zinc acetate dihydrate and *n*-propyl amine, were purchased from Aldrich Chemical Co. Ltd and used without further purification. The pH of the prepared solution was observed at 8.39 using a pH meter (Cole parmer, U.K). The mixture of zinc acetate dihydrate ($Zn(AC)_2 \cdot 2H_2O$, 0.3 M) and *n*-propyl amine was transferred to a three necked flask and was refluxed at ~65 °C for 9 h. After completion of the reaction, the white product formed was air cooled at room temperature. The white product was transferred to a centrifugation tube to remove the organic synthetic impurities *via* a centrifugation process (4000 rpm min^{-1} for 10 min, FLETA 5, Hamlin Sci ind. co. Ltd, U.K). The white product obtained was washed repeatedly with alcohol (methanol (MeOH), ethanol (EtOH)) and acetone, and dried in a petridish at room temperature.

Characterization of the ZnO-QDs

The dried white powder sample was characterized in terms of its structural and chemical properties. The structural observations of the white powder were made using field emission scanning electron microscopy (FESEM, Hitachi S-4700, Japan) and transmission electron microscopy (TEM, 200 keV, Jeol JSM 2010, Japan). The crystallinity and phases of the white powder were characterized using X-ray powder diffraction (XRD, Rigaku, Japan) with CuKα radiation ($\lambda = 1.54178$ Å) in range of 20°–65° with 6° min^{-1} scanning speed.

XRD (Fig. S1(a)†) shows the diffraction peaks in the pattern indexed as the hexagonal zinc oxide with lattice constants $a = 3.249$ and $c = 5.206$ Å, and well matched with the accessible Joint Committee on Powder Diffraction Standards (JCPDS card no. 36-1451) of the formed QDs. The particle size of the grown QDs was also calculated using the well-known Scherrer formula with the FWHM of XRD pattern and the value of the major peaks such as ⟨1010⟩, ⟨0002⟩, ⟨1011⟩, ⟨1012⟩, ⟨1120⟩, and ⟨1013⟩ obtained at 32.08°, 34.82°, 36.65°, 47.94°, 57.00° and 63.26°, respectively (ESI, Table S1†) and shows that the dimension of particles were very small.[25–27]

$$D = \frac{0.9\lambda}{\beta \cos\theta}$$

where λ is the wavelength of the X-ray radiation source, β is full-width at half-maximum [FWHM] in radians, and θ is the Bragg's diffraction angle. The calculation was measured with the help of Gaussian Lorentzian fitting program. The mean value of the particle sizes is ~7–8 nm. The chemical functional properties of the white powder of grown QDs was characterized by Fourier transform infrared spectroscopy (FTIR, Perkin Elmer, U.S.A) in the range of 4000–400 cm^{-1}. In addition to these observations, the optical properties of the QDs were also analysed at room temperature *via* UV-visible (Labomed, Model UV D-2950, in the range of 200–1000 nm) and photoluminescence (PL) spectroscopy using the He-Cd (325 nm) laser line as the exciton source in the range between 350 and 650 nm.

Binding studies of ZnO-QDs with HSA protein

Binding studies of HSA with ZnO-QDs. The fluorescence quenching titration at an increasing HSA to ZnO-QDs molar ratio was performed. Briefly, at a fixed concentration of HSA

(3 μM), various concentrations of ZnO-QDs (5–50 μM) were added in 10 mM Tris–HCl buffer at ambient temperature. The fluorescence spectra were obtained under subdued light. Fluorescence measurements were carried out on a Shimadzu spectrofluorophotometer (model RF5301PC) equipped with RF 530 XPC instrument control software using a quartz cell of 1 cm path length. The excitation and emission slits were set at 3 nm and 10 nm, respectively. The excitation and emission wavelengths at which the HSA fluorescence was obtained were 280 nm and 330 nm, respectively. ZnO-QDs alone don't exhibit fluorescence in this wavelength range. Fluorescence quenching in terms of the quenching constant was determined following the Stern–Volmer equation.[28] The slope of the double-logarithm plot $\log[(F_0 - F)/(F - F_\infty)]$ *versus* log[ZnO-QDs] in the linear range provided the number of equivalent binding sites (n); however, the value of log[ZnO-QDs] at $\log[(F_0 - F)/(F - F_\infty)] = 0$ is equal to the negative logarithm of the binding constant (K_a).[28,29]

Cell culture

The cancer cells (C2C12) were procured from American Type Culture Collection (ATCC-CRL 1772; Bethesda, MD) and thawed at 37 °C in a water bath for ~2–3 min. The thawed cells were mixed with Dulbecco's modified eagle's medium (DMEM) and centrifuged for 4 min. The supernatant solution was discarded from the centrifuge tube and the cells were transferred to a 75 mm^2 area of volume bottles and were cultured in growth medium DMEM containing 10% fetal bovine serum (FBS) with antibiotics (streptopenicillin and amphotericin B solution, 10 mL L^{-1} each, sigma) in a humidified incubator at 37 °C under a 5% CO_2 and 95% O_2 environment and washed with dulbecco's phosphate buffer (DPBS) solution. The medium was refilled every other day and the number of cells was observed daily and counted using a haemocytometer and subcultured after reaching 50% confluence.

In vitro cell growth inhibition assay (MTT assay)

The MTT assay was used to check the percentage of viable cells *via* cell proliferation kit I (MTT, provided by ROCHE, Ltd, U.S.A) as per the detailed directions. Briefly, the cell lines were seeded into 96-well plates at 5×10^3 cell per well and incubated overnight at 37 °C in a humidified incubator. The C2C12 cells were incubated with different concentrations of ZnO-QDs and returned to the incubator for 24, 48, 72 and 96 h. The MTT (3-(4,5-dimethyl thiazol-2-yl)-2,5-diphenyl tetrazolium bromide) solution (10 μL per well) was mixed with DMEM. The stored MTT stock solution was added to the control and treated with ZnO-QDs cell samples and again incubated at 37 °C for 4 h. After incubation, the samples were removed from incubator and mixed with solubilizing buffer (100 μL per well) solution, a purple color visible at this stage and deepened over pipetting. The control and treated samples were again incubated overnight to ensure the formazan precipitate was dissolved. Measurement of the MTT assay was performed with an Elisa Reader (Bio-Rad) at 570 nm. The UV-irradiation was provided by the deuterium and Xenon lamp. The percentage (%) of viable cells can be calculated as follows:

% viability = [(total cells - viable cells)/total cells] × 100

Or

% viability = OD (optical densities) in sample well/OD in control well × 100

MTT Assay

Seeding of cells in 96-well plate (5×10^3 cells per well)

↓ 24 h

Treatment of cells with prepared ZnO-QDs

↓ 24 h

Add MTT solution (10–20 μL to each well)

↓ 3 h

Discard media and add solubilizing buffer solution (100 μL) to each well

↓ Store overnight in 37 °C incubator

Read at 570 nm (ELISA reader) or store plate at -20°C

Measurement of reactive oxygen species (ROS)

Intracellular production of ROS was measured using 2,7-dichlorofluorescein diacetate (DCFH-DA) as described by Wang and Joseph.[30] The DCFH-DA passively enters the cell, wherein it reacts with ROS to form the highly fluorescent compound, dichlorofluorescein (DCF). In brief, a 10 mM DCFH-DA stock solution (in MeOH) was diluted in culture medium without serum or another additive to yield a 100 μM working solution. C2C12 cancer cells were treated with ZnO-QDs at different concentrations (10, 100 and 200 μg mL^{-1}) for 24 h. At the end of exposure, the cells were washed twice with buffer and then incubated in 1 mL of the working solution of DCFH-DA at 37 °C for 30 min. Cells were centrifuged for 10 min and 200 μL of the supernatant was transferred to a 96-well plate. The fluorescence intensity was recorded at an excitation wavelength of 485 nm and emission wavelength of 525 nm.

Confocal microscopy (CSLM) measurement

For quantitative study related to C2C12 cells and QDs, the cells were grown into a specialized confocal disk at 5×10^3 cell per well and incubated with QDs for different incubation periods (24, 48, 72 and 96 h) at 37 °C in a humidified environment. When the cells were reached at 50% confluence, the media was removed from the confocal disk and DPBS (200 μL) solution added, shaken and the DPBS removed from the confocal disk. The cells were fixed with using ethanol (70%, 200 μL) for 10 min to achieve complete fixation. The incubated cells were again washed with DPBS and shaken and the media was completely removed from the disk. Furthermore, the cells were stained with propidium iodide [PI] (50 μL (PI) + 150 μL (DPBS)] solution and again incubated at 37 °C for 30 min in an incubator and washed with DPBS buffer. The stained cells were covered with a glass cover slip for microscopic observation.

Total RNA extraction from cultured C2C12 cells

Total RNA was extracted from C2C12 cells after various treatments for set periods of time using Trizol (sigma) according to the manufacturer's protocol. The purity of the total RNA was assessed by the ratio of the optical density at 260–280 nm (acceptable values being between 1.6 and 2.1). First strand cDNA was synthesized from 1 μg of the total RNA using M-MLV reverse transcriptase with the anchored oligo d(T)12-18 primer. Real-time PCR was performed using a cDNA equivalent of 10 ng of total RNA from each sample with primers specific for caspase 3 and caspase 7 genes with a housekeeping gene GAPDH (ESI, Table S2†). The reaction was carried out in 10 μL using Sso-FastTM EvaGreen®Supermix (Bio-Rad) according to the manufacturers' instructions. Relative ratios were calculated based on the $2^{-\Delta\Delta CT}$ method.[31] PCR was monitored using the CFX96TM Real-Time PCR Detection Systems (Bio-Rad) (for detailed information, please see the ESI†).

Statistical analysis

The obtained data are expressed as the mean ± SD. Statistical analysis was performed using student *t*-tests. The results were considered significant when $p < 0.05$.

Results

Morphological invistigation

Detailed investigations of the synthesized ZnO-QDs in terms of their morphology and crystalline quality have been performed and the corresponding observations are demonstrated (Fig. 1). Fig. 1(a) and (b) illustrate the low and high magnified FESEM images of the QDs. It is very clear from the FESEM images that the ZnO-QDs are having spherical shape with gathered form and a closer look reveals their diameters to be in the range of 7–8 nm. To confirm the morphology and crystalline quality, the ZnO-QDs were investigated in detail inside TEM and their corresponding observations are demonstrated in Fig. 1(c) and (d). In agreement with the FESEM results, TEM observations also confirmed that these QDs exhibit almost spherical geometry with diameter about 7–8 nm (Fig. 1(c)). The HR-TEM investigations (Fig. 1(d)) on these ZnO-QDs confirmed their hexagonal wurtzite crystal structures with a lattice constant of around 0.265 nm (a axis), which was also found to be consistent with the selected area electron diffraction (SAED) studies (inset of Fig. 1(d)). Both the TEM and FESEM observations are consistent with the XRD analysis and denote that the synthesized QDs are single crystalline in nature (ESI, Fig. S1a†).[25–27] Because several chemicals were involved during their synthesis, the ZnO-QDs were studied using FTIR spectroscopy to investigate if any chemical residues remained after the synthesis process. The FTIR spectrum (Fig. 1(e)) confirms the fingerprints of $Zn(Ac_2).2H_2O$ and *n*-propylamine, which were used to synthesize the ZnO-QDs. The large and shallow peak range from 3200 to 3600 cm^{-1} and corresponds to the water molecules, whereas the sharp peaks centered at 1585 cm^{-1} and 1405 cm^{-1} are associated with C=O stretching from zinc acetate.[32–35] A curved

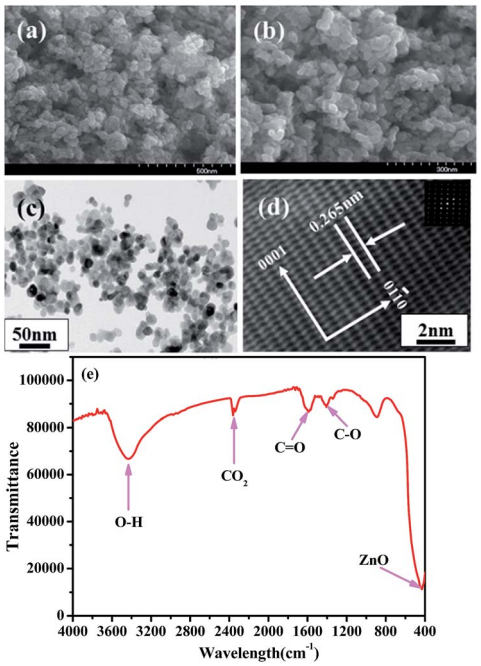

Fig. 1 FESEM images of the grown ZnO-QDs: (a) low magnification images and (b) high magnification images. (c) The low magnification TEM image of the grown ZnO-QDs. (d) The HR-TEM image showing the difference between the two lattice fringes, which is ~0.265 nm. The corresponding SAED pattern (inset) is consistent with the HR-TEM observations and indicates the single crystallinity of the synthesized product. (e) The FTIR spectrum of the grown ZnO-QDs.

and flat peak around 433 cm^{-1} in the FTIR spectrum represents the formation of the ZnO-QDs.

The ZnO-QDs were dispersed in deionized water (DW) and their corresponding UV-visible spectrum (ESI, Fig. S1b†) shows a broad band absorption around 362 nm (3.42 eV), near to the 1s–1s electron transition (3.37 eV) from ZnO-QDs.[32–35] Furthermore, the luminescent properties of the ZnO-QDs (at room temp) were investigated using PL spectroscopy and their corresponding PL spectrum is presented (ESI, Fig. S1c†). A very sharp and intense PL peak was observed at around 398 nm in the UV region, which is mainly due to excitons; however, no peak was observed in the green region confirming the high quality of these ZnO-QDs.[36] Normally, a green peak is also expected in the PL spectrum due to the presence of oxygen vacancies on the surface but in present case it seems that the oxygen vacancies are passivated due to used chemicals during the synthesis.[36–41] To utilize them for cancer studies, it was very necessary to investigate the different properties of the ZnO-QDs and all the observations confirmed that these QDs exhibit very high crystalline qualities.

Based on the synthesis, characterization and observations of the prepared QDs, a chemical formation process is also projected for the QDs. As per the material and methods, once $Zn(AC)_2 \cdot 2H_2O$ is mixed in solution with *n*-propylamine under incessant stirring in MeOH, it forms a clear solution without precipitation at pH 8.39. Subsequently, six hours of reflux at 65 °C, a white product forms in the refluxing pot and the refluxing process was completed in nine hours. As per the chemical observations

(Fig. 1(e)), the amine ($-NH_2$) group decays out from *n*-propylamine due to the breaking of hydrogen bonds and it reacts with the acetate (CH_3COO^-) group of $Zn(AC)_2 \cdot 2H_2O$ initially (eqn (1)), and the Zn^{2+} ions react with the propyl group to form a zinc complex ($ZnN-(CH_2)_2-CH_3$). It is assumed that as the temperature increases during the refluxing step, the hydroxyl (OH^-) ions from MeOH react with the zinc complex and Zn^{2+} ions from the complex decompose, which then react to the hydroxyl (OH^-), form zinc hydroxide ($Zn(OH)_2$) (eqn (2)), which is converted into pure zinc oxide at higher refluxing temperature (ZnO) with water molecules (eqn (3)). The intermediate species ($(CH_3)_2N-(CH_2)_2-CH_3$, CH_3COOH and H_2O molecules) from the reaction was pass out during centrifugation of the product.[32–35]

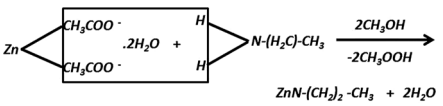

(1)

$$ZnN-(CH_2)_2-CH_3 + 2H_2O + 2CH_3OH \xrightarrow{\text{at increased refluxing temperature}} (CH_3)_2N-(CH_2)_2-CH_3 + Zn(OH)_2 + 2H_2O \quad (2)$$

$$Zn(OH)_2 \rightarrow ZnO + 2H_2O \quad (3)$$

The interaction between HSA and ZnO-QDs was assessed at different concentrations, notable by the fluorescence technique Fig. 2. The fluorescence emission spectra were obtained in ranges from 5 μM to 50 μM in five steps at 330 nm. In addition to an increase in the concentration of ZnO-QDs, the fluorescence intensity gradually decreased, after the quenching process HSA binds with ZnO-QDs and the fluorescence quenching constant (K_{sv}) was calculated using the Stern–Volmer equation (eqn (4)) as follows:[28]

$$F_0/F = 1 + K_{sv}\,[\text{ZnO-QDs}] \quad (4)$$

where F_0 is absence fluorescence intensity, F is the presence fluorescence intensity and K_{sv} is the Stern–Volmer quenching constant. A plot was established between F_0/F *versus* [ZnO-QDs] (data not shown), which obtained the fluorescence quenching constant ($K_{sv} = \sim 4.5 \times 10^4$ L mol^{-1}) using the slope of the straight line. The linear line graph expressed that only one way quenching track, for example, static quenching or dynamic quenching, was observed.[42] For the applied eqn (5), the bonded macromolecules set independently after reaching an equilibrium point (at free and bound molecules). Moreover, when the molecules bind independently to a set of equivalent sites on a macromolecule, the equilibrium between the free and bound molecules is given by the equation as follows:[28]

$$\log[(F_0 - F)/F] = \log K + n \log[Q] \quad (5)$$

where K is the binding constant. Thus, a plot of $\log(F_0 - F)/F$ *versus* log[ZnO-QDs] can be used to determine K.

In the culture process, proliferation of the C2C12 cells interacted with ZnO-QDs at regular interval incubation times (24, 48, 72 and 96 h) occurred. Hereafter, most cells are single nucleates or mononucleate after the first day and on the third day, the cells reached a 50% confluence (ESI, Fig. S2†). Moreover, the accommodated cells are directly connected with the ZnO-QDs, which indicates the exact condition of the cells, as increasing the concentration of ZnO-QDs (10, 100 and 200 μg mL^{-1}) increases the mortality of the cancerous cells due to the strong interactions between the C2C12 cells and the ZnO-QDs.

The MTT assay was used to examine the rate of proliferation of cells and toxicity caused using the ZnO-QDs in cancer cells. This happens due to mitochondrial damage in the cells and therefore decreased the efficiency in test. The MTT salt, which has yellow colour solution, reduces to purple formazan in the mitochondria of living cells. To dissolve or solubilize a buffer solution DMSO is usually added to the insoluble purple formazan product to form a coloured solution. The absorbance of this colored solution was quantified by measuring at a certain wavelength (usually 570 nm) using a spectrophotometer. The absorption maximum mainly depends on the solvent employed. The level of cytotoxicity or the percentage (%) viability was calculated as follows:

$$\text{Viability} = [(\text{total cells} - \text{viable cells})/\text{total cells}] \times 100$$

The acquired MTT assay information showed that various ZnO-QDs concentrations exhibit constrained properties on the evolution of C2C12 cells. For endurance studies, cells were

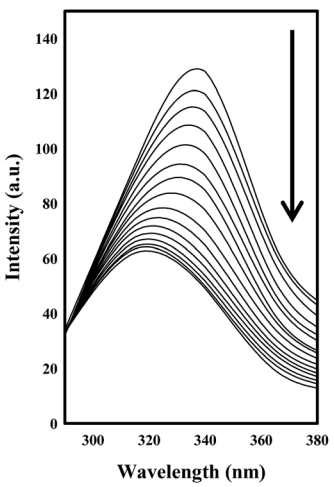

Fig. 2 The illustrative fluorescence spectra of the ZnO-QDs in the absence and presence of various concentrations of HSA, which shows the emission spectra of the ZnO-QDs (50 μM) upon varying the HSA concentration, *i.e.*, 5, 10, 15, 20, 25, 30, 35, 40, 45 and 50 μM.

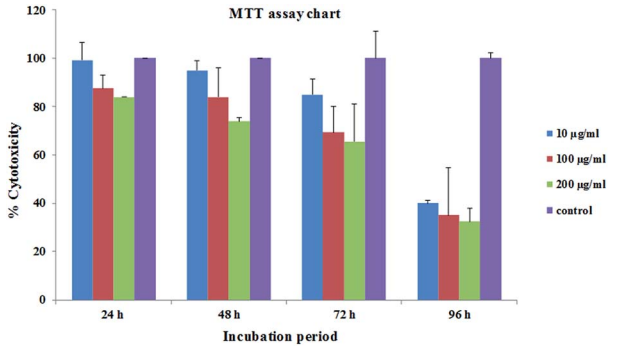

Fig. 3 MTT assay chart after different incubation periods (24, 48, 72 and 96 h) with the control solution.

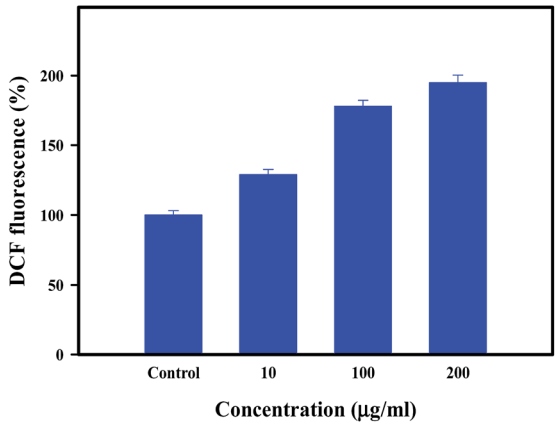

Fig. 4 The induced oxidant generation in C2C12 cancer cells treated with various concentrations of ZnO-QDs (control, 10, 100 and 200 μg mL^{-1}) incubated for 24 h.

incubated with ZnO-QDs continuously and thereafter the media were removed and the cell density was determined *via* the MTT assay following the addition of 10, 100 and 200 μg mL^{-1} of ZnO-QDs solution.[43–45] The ZnO-QDs at a concentration of 10, 100, and 200 μg mL^{-1} after 24 h killed 15.96%, 12.53% and 0.79%, respectively, and for 48 h of incubation, the cell decay behaviour was changed to 26.11%, 15.97% and 5.12% for the same ZnO-QDs concentrations (*i.e.*, for 10, 100 and 200 μg mL^{-1}), respectively. As the evolution time of the cells increases in terms of the desired concentration of ZnO-QDs, the cell death occurred corresponding to 72 h of incubation was 34.53%, 30.65% and 15.05% for 10, 100 and 200 μg mL^{-1} of ZnO-QDs solution, respectively. The ZnO-QDs at concentrations of 10, 100 and 200 μg mL^{-1} killed the maximum number of cells, which were 67.55%, 64.94% and 59.94%, respectively (Fig. 3).

The ZnO-QDs used in the present study considerably transformed the prominence factor in terms of oxidant in the C2C12 cancer cells. A higher production of intracellular reactive oxygen species (ROS) in the ZnO-QDs treated cancer cells suggests that ROS generation and oxidative stress might be the primary mechanisms responsible for the induced toxicity cancer cells due to the ZnO-QDs. Current developments in cancer research suggest that a number of apoptotic stimuli share common mechanistic pathways characterized by the generation of ROS through oxidative stress.[46,47] ROS typically include the superoxide radical ($O_2^{\bullet -}$), hydrogen peroxide (H_2O_2), and hydroxyl radical ($^{\bullet}OH$), which can cause damage to cellular components, including DNA and proteins. The induced oxidative stress was evaluated with various concentrations of ZnO-QDs (0, 10, 100 and 200 μg mL^{-1}) incubated for 24 h (Fig. 4). At the end of treatment, the ROS levels were determined, as described in the materials and methods section. The ROS data are represented as the mean ± standard deviation of three identical experiments. The qualitative analysis of ROS generation revealed a concentration dependent increase of 129%, 178%, and 195% at 10, 100 and 200 μg mL^{-1}, respectively, in the fluorescence intensity of DCF in ZnO-QDs treated cells compared to the untreated control cells (Fig. 4). Considering the fluorescence intensity of the untreated control cells as 100%, the ZnO-QDs treated cells (in the concentration range of 0–100 μg mL^{-1}) were found to exhibit significantly higher fluorescence intensity of DCF ($p < 0.005$).[46,47]

Furthermore, cell death with the QDs was studied in detail using time dependent confocal scanning laser microscopy (CLSM) at different concentrations of the ZnO-QDs with the control solution. The CLSM provides information on the cells behaviour in a wet environment. The cells were incubated with the QDs at 37 °C in an incubator with 5% CO_2 for 24, 48, 72 and 96 h, imposed using a CLSM with the staining solution PI and were observed with an excitation at 543 nm and emission at 620 nm (ESI, Fig. S3†). It was observed that the density of cell death after 24 h of incubation was less (10 μg mL^{-1}) (Fig. 5), which increased with an increase in the concentration of ZnO-QDs from 100 μg mL^{-1} to 200 μg mL^{-1}.

In addition with an increase in incubation time (48 h), the cell death density was enhanced more and more, which is shown in Fig. 5(a)–(h). It is very clear from the CLSM images that the toxicity of the cells mainly depends on the concentration of QDs

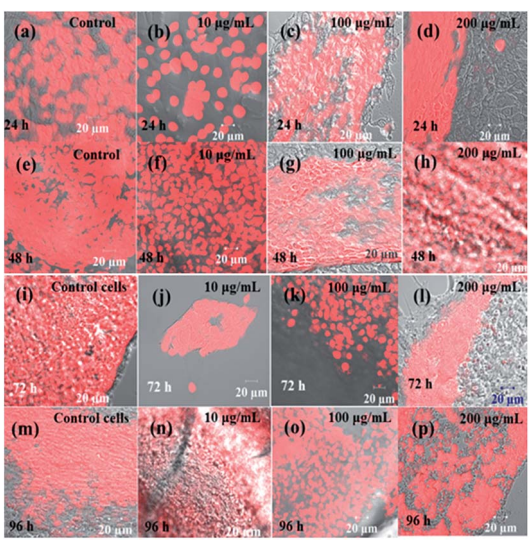

Fig. 5 Confocal laser scanning microscopy (CLSM) images of C2C12 cells at different concentrations of ZnO-QDs (10, 100 and 200 μg mL^{-1}) with altered evolution periods (24, 48, 72 and 96 h).

and also with the incubation period.[48,49] From the CSLM observations, which are in close agreement with the MTT assay data (Fig. 3 and ESI, Fig. S3†) and from both, it is very clear that the several hundred thousands of cells are accumulated in a spherical shape and the addition of the ZnO-QDs significantly decreased the density of cancerous cells (Fig. 5). The control cells show the density of C2C12 cells (Fig. 5), but as the dose of QDs was increased in dose dependent (10, 100 and 200 μg mL^{-1}) and an optimized manner, the cell density decreased. However, the detailed mechanism and cause of the induced toxicity in the cancerous cells due to the QDs is still under debate and needs further experimental studies, which are under progress.

The previous cytotoxicity study with cancer cells with zinc oxide nanoparticles carried out by Wahab *et al.*, strongly suggested that the exposure of C2C12 cells to NPs from lower to higher concentrations (5–100 μg mL^{-1}), respectively, incubated at 37 °C for 24 h, affects the cell growth by increasing the concentration of NPs.[49] The present study is analogous to our previous study.[49] In another study, gold nanoparticles decreased the growth of C2C12 cells in a dose dependent manner at very low concentrations (0, 100, 500, 1000 ng mL^{-1}) incubated for 24 h at 37 °C.[50] The mechanism of cell death was also explained with the utilization of CuO quantum dots on candidate genes such as caspases 3/7, which are responsible and key factors in apoptotic functions. The *in vitro* study of C2C12 with QDs described the effects on DNA, which significantly decrease the viability of cells in a dose dependent manner (10–20 μg mL^{-1}).[51] On the basis of microscopy and previous published results, it can be summarized that the cytological potential of the prepared QDs has remarkable significance in this study at the optimized concentration range.[51]

The RT-PCR investigation was performed to deduce the level of mRNA with markers (caspase 3/7) in the presence of GAPDH gene against C2C12 cells. The cancer cells were interacted with QDs at low (10 μg mL^{-1}) and high concentrations (200 μg mL^{-1}) of QDs after incubation periods of 24 and 72 h. The obtained outcomes showed that mRNA levels of markers (caspase 3/7) were significantly changed in C2C12 cells due to the QDs interactions (Fig. 6, $p < 0.05$ for each). Genes expressions for caspase 3 with ZnO-QDs at low concentrations after different incubation periods (24 and 72 h) were 1.4 and 2.1, respectively. In the case of caspase 7, the change of expression was upregulated 2.7 fold after 24 h, whereas it was 4.7 fold higher after 72 h of incubation. The quantifiable RT-PCR outcomes revealed that the QDs show an up-regulated mRNA level for the cell cycle checkpoint of caspase 3/7.[31] The influence of caspases 3/7 was noticed in the control cells, which resembled naturally growing cells due to incubation or aging. In the reacted cells, the activities of caspase 3/7 improved from 1.4 to 4.7 fold ($p < 0.05$) over the basal levels, which signifies an initiation of caspases in C2C12 cells reacted with QDs.[31] The change in gene expression was compared with an untreated sample as a control or a signature control for the knockdown data. From the statistical graph (Fig. 6), it is very clear that the ZnO-QDs exhibit a toxic nature with respect to the growth of cancer cells. The apoptosis in the cell was increased as the concentration of QDs increased. The up regulation denotes the apoptosis caused due to the interaction of QDs. Similar observations have been obtained in case of caspase 7 interactions after 24 and 72 h of incubation. In case of caspase 7 gene expression, at a low concentration of ZnO-QDs incubated for 24 h, a two-fold change (2.0, 2.1 for 24 h incubation periods) in apoptosis was observed, whereas at the higher concentration and higher incubation period (72 h), apoptosis changes 6 fold (6.6) (Fig. 6).

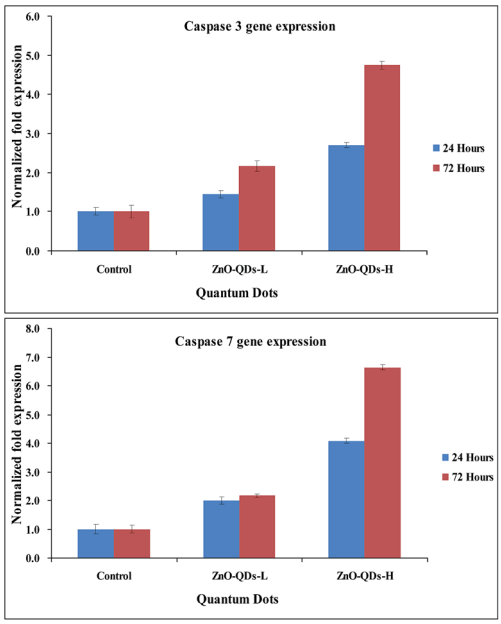

Fig. 6 mRNA expression of C2C12 cells with caspase 3/7 and housekeeping GAPDH genes in the presence of ZnO-QDs at low (10 μg mL^{-1}, ZnO-QDs-L) and high (200 μg mL^{-1}, ZnO-QDs-H) concentrations. The experiments were performed in triplicate ($p < 0.05$).

Discussion

The synthesis of QDs (<10 nm) from a precursor of ZnO is a very important aspect because they exhibit potential industrial applications in various technical areas such as solar cells, UV light emitters, gas/chemical sensors, transparent conductors, and optoelectronics. Recently, the utilization range of ZnO-QDs has been expanded to biomedical engineering because of their large *S*/*V* ratio, enhanced catalytic, and biocompatibility.[14,32–35] Their very small nanoscale size makes them noticeable and valuable material for further biorelated applications, for example in drug delivery, cell and DNA repair/damage.[6,7,14,32–35] The ZnO-QDs in the present study were prepared *via* a non-aqueous solution process. The XRD results confirmed that they are single crystalline in nature and their dimension are in the quantum size range (<10 nm). TEM revealed their nearly spherical shape and smooth surface, and the average diameter was about 7–8 nm in agreement with the XRD analysis. The HR-TEM study also supported their crystalline nature with an average lattice spacing of ~0.265 nm, which is identical to pure wurtzite ZnO.[6,7,14,32–35] The toxicity of the grown QDs in a cultured medium of cancer cells was determined using MTT assay analysis. From the detailed observation of the MTT assay,

it is clear that these small ZnO-QDs (diameter ~7–8 nm) exhibit a remarkable effect against C2C12 cells (at low doses of 10, 100 and 200 μg mL^{-1} in a dose dependent manner) in presence of the control solution.[52] The cell toxicity was also observed in terms of apoptosis and cell death due to the QDs and was also observed with the existence of ROS in a dose dependent manner (for an incubation time of 24 h). The apoptosis in C2C12 cells were analysed *via* RT-PCR utilized to analyse the mRNA levels of apoptotic markers (*e.g.* caspase-3/7) in presence of the QDs at low and high (10 μg mL^{-1} and 200 μg mL^{-1}) concentrations for 24 h incubation. The observed expression data in both cases (caspase-3/7 with ZnO-QDs) were accordingly up-regulated.[53] In the recent past, previous studies show that cytochrome c binds to the protease of apoptosis, which is generally known as the apoptosis of protease activating factor-1 (Apaf-1) and forms a complex apoptosome. These apoptosomes have the property to bind with procaspase-7 and causes their auto-activation through a conformational change. As caspase-7 is initiated, it goes on to activate caspase-3, cleaves the substrates at their aspartate residues and activation of this proteolytic activity leads to apoptosis. The RT-PCR study supports that the QDs are significantly up-regulated with caspases-3/7 expression in proliferated cells.[54–56] On the basis of the findings and their observations, we have proposed a probable pictorial model for the cytotoxic process of ZnO-QDs with C2C12 cells, which is shown in Fig. 7.

On the basis of the previous literature[45] and observations, it can be postulated that the cytotoxicity caused by QDs/NPs depends on various parameters such as size, shape, chemical structure, and stoichiometry of the QDs. The toxicity *via* QDs also affects the endocytic uptake of cells.[57] The QDs first attach on the surface of cancerous cells, which exhibit small pores. These pores form passages to enter the QDs on cancer cells (Fig. 7). Due to very small size of QDs, they exhibit the natural tendency to cross the upper layers of cancerous cells very easily compared to other bigger size nanostructures. It is assumed that in cells, QDs are joined with other particles and form aggregates and these aggregates of QDs are responsible for the destruction of cell organelle, for instance the nucleus, which has a ~5–10 μm size and mitochondria, endoplasmic reticulum and nucleic acids (~1–2 μm).[45,46] From the gene expression data (Fig. 6), it is very clear that the introduced QDs are responsible for controlling the proliferation and destruction of the cell organelle in cancer cells. The dose dependent MTT and RT-PCR studies clearly demonstrate the apoptosis and cell death in cancer cells. The treatment also explains to sensitize C2C12 cells, by increasing the concentration of ZnO-QDs. The increased cell death is caused by the dose dependent addition of ZnO-QDs after different incubation periods (ESI, Fig. S3,† Fig. 4). From the genetic (RNA extraction) studies (Fig. 6), it is evident that cell growth is significantly affected in presence of ZnO-QDs, which are mainly responsible for cell death. The cytotoxicity of the grown materials of ZnO-QDs was tested with an MTT assay in the grown cultured system.[44] The free radicals (FRs), which are generally produced in cultured cells interact *via* the solution of nanostructured materials, are responsible for the generated ROS. These FRs have the property to enter into the outer wall of the cells and go into the inner wall of cell membrane. In cells enzymatic changes occurred when the FRs react with the cells organelle, which leads to damage or the disorganization of cells.[45,49,57] The previous study highlight that the nanostructures have the capability to induce ROS in cancer cells.[49] The mRNA levels of expression of caspase-3/7 in presence of ZnO-QDs in cancer cells have been examined. The RT-PCR results showed that the QDs, up-regulate the mRNA level of the cell cycle checkpoint. The mRNA expressions and their actions on apoptotic gene caspase-3/7 were higher in the QDs treated cells. The phenomena why the QDs are responsible for decreasing the proliferation rate of cells and their biochemical and enzymatic changes are under investigation and needs further study to investigate the role of QDs against cancer cells.[57] In most of the published literature, the nanostructures employed either utilized toxic material or were used at higher concentrations for the toxicity studies, which are undesirable for human exposure. We may believe that the use of small sized structures (QDs of ZnO) at optimized/low concentrations would be supportive to control the explosion of cancer cells due to their biocompatible nature and have no adverse effects on the body.[58]

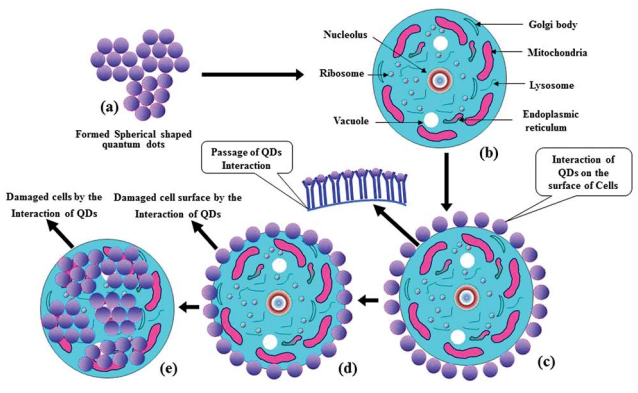

Fig. 7 A schematic of the proposed mechanism of the interaction of ZnO-QDs against C2C12 cells and their cytological death.

Conclusions

In summary, the high crystalline qualities of ZnO-QDs with very uniform size distribution were successfully synthesized *via* a solution process in a controlled manner. The synthesized ZnO-QDs were utilized for investigating their effect with respect to cancer cells (C2C12) and the results suggest that these QDs may be regarded as an effective new class of anticancer agent. We found that the lower concentration of utilized QDs has a much more pronounced effect in comparison to larger amounts of QDs. The low concentrated ZnO-QDs seem to easily enter into the cells pores and react significantly with the cells organelles; however, when a large concentration of QDs is utilized, self-agglomeration of QDs might hinder their effective entry into the cells and therefore reduce their effects. The MTT, ROS and RT-PCR studies clearly demonstrate that the treatment of QDs in a dose dependent manner against C2C12 cells

decreases the growth of cancer cells. The main importance of our findings shows that the QDs of ZnO can be utilized as an effective anticancer agent at low concentrations. However, a detailed investigation relating to the structure and activity of the QDs, as well as their stability in cells under appropriate conditions are required. The comprehensive observations might be helpful in designing more effective anticancer agents for therapeutic use. From these studies, it is confirmed that the QDs are safe and effective candidates to reduce the growth of cancer cells for large scale applications. The apoptosis correlated ROS production was also quantified in C2C12 cancer cells with QDs at various doses. The genetic caspase studies also revealed that the cell growth is strongly affected due to ZnO-QDs, which are responsible for cell death.

Conflict of interest

The authors declare that there are no conflicts of interest.

Acknowledgements

This study was financially supported by the King Saud University, Vice Deanship of Research Chairs.

References

1 X. Michalet, F. F. Pinaud, L. A. Bentolila, J. M. Tsay, S. Doose, J. J. Li, S. Sundaresan, A. M. Wu, S. S. Gambhir and S. Weiss, *Science*, 2005, **307**, 538–544.
2 K. Riehemann, S. W. Schneider, T. A. Luger, B. Godin, M. Ferrari and H. Fuchs, *Angew. Chem., Int. Ed.*, 2009, **48**(5), 872–897.
3 Y. K. Mishra, R. Adelung, C. Röhl, D. Shukla, F. Spors and V. Tiwari, *Antiviral Res.*, 2011, **92**(2), 305–312.
4 T. E. Antoine, Y. K. Mishra, J. Trigilio, V. Tiwari, R. Adelung and D. Shukla, *Antiviral Res.*, 2012, **96**, 363–375.
5 H. Papavlassopoulos, Y. K. Mishra, S. Kaps, I. Paulowicz, R. Abdelaziz, M. Elbahri, E. Maser, R. Adelung and C. Rohl, *PLoS One*, 2014, **9**(1), e84983.
6 R. Wahab, N. K. Kaushik, N. Kaushik, E. H. Choi, A. Umar, S. Dwivedi, J. Musarrat and A. A. Al-Khedhairy, *J. Biomed. Nanotechnol.*, 2013, **9**, 1181–1189.
7 R. Wahab, N. K. Kaushik, A. K. Verma, A. Mishra, I. H. Hwang, Y. B. Yang, H. S. Shin and Y. S. Kim, *J. Biol. Inorg. Chem.*, 2011, **16**(3), 431–442.
8 Y. Weizmann, F. Patolsky, E. Katz and I. Willner, *J. Am. Chem. Soc.*, 2003, **125**, 3452–3454.
9 H. T. Song, J. S. Choi, Y. M. Huh, S. J. Kim, Y. W. Jun, J. S. Suh and J. W. Cheon, *J. Am. Chem. Soc.*, 2005, **127**(28), 9992–9993.
10 M. Mahmoudi, A. Simchi, M. Imani and U. O. Hafeli, *J. Phys. Chem. C*, 2009, **113**(19), 8124–8128.
11 J. M. Laval, P. E. Mazeran and D. Thomas, *Analyst*, 1999, **125**, 29–33.
12 T. A. Desai, *Med. Eng. Phys.*, 2001, **22**(9), 595–606.
13 R. H. Hurt, M. Monthioux and A. Kane, *Carbon*, 2006, **44**(6), 1028–1033.
14 R. Wahab, Y. S. Kim and H. S. Shin, *Curr. Appl. Phys*, 2011, **11**, 334–340.
15 H. H. Wang, C. S. Xie, W. Zhang, S. Z. Cai, Z. H. Yang and Y. H. Gui, *J. Hazard. Mater.*, 2007, **141**, 645–652.
16 S. S. Hong, T. H. Joo, I. I. W. Park, Y. H. Jun and G. C. Yi, *Appl. Phys. Lett.*, 2003, **83**, 4157–4159.
17 D. Bechet, P. Couleaud, C. Frochot, M. L. Viriot, F. Guillemin and M. B. Heyob, *Trends Biotechnol.*, 2008, **26**, 612–621.
18 T. Jamieson, R. Bakhshi, D. Petrova, R. Pocock, M. Imani and A. H. Seifalian, *Biomaterials*, 2007, **28**, 4717–4732.
19 K. Y. Kim, *Nanomedicine*, 2007, **3**, 103–110.
20 Y. Chen, D. M. Bangall, H. Koh, K. P. Hiraga, K. Z. Zhu and T. Yao, *J. Appl. Phys.*, 1998, **84**, 3912–3918.
21 G. M. Murphy, *Photodermatol., Photoimmunol. Photomed.*, 1999, **15**, 34–36.
22 W. C. Earnshaw, L. M. Martins and S. H. Kaufmann, *Annu. Rev. Biochem.*, 1999, **68**, 383–424.
23 M. Enari, H. Sakahira, H. Yokoyana, K. Okawa, A. Iwamatsu and S. Nagata, *Nature*, 1998, **391**(6662), 43–50.
24 H. Sakahira, M. Enari and S. Nagata, *Nature*, 1998, **391**(6662), 96–99.
25 Q. Zhang, T. P. Chou, B. Russo, S. A. Jenekhe and G. Z. Cao, *Angew. Chem., Int. Ed.*, 2008, **47**(13), 2402–2406.
26 G. Ambrožič, S. D. Škapin, M. Zigon and Z. C. Orel, *J. Colloid Interface Sci.*, 2010, **346**(2), 317–323.
27 B. D. Cullity, *Elements of X Ray Diffraction*, Addison-Wesley, Reading MA, 1978, p. 102.
28 J. R. Lakowicz, *Principles of Fluorescence Spectroscopy*, Springer, 3rd edn, 2006, pp. 278–282.
29 K. L. Henderson, I. B. Belden and I. R. Coats, *Environ. Sci. Technol.*, 2007, **41**, 4084–4089.
30 H. Wang and J. A. Joseph, *Free Radical Biol. Med.*, 1999, **27**, 612–616.
31 M. W. Pfaffl, *Nucleic Acids Res.*, 2001, **29**(9), e45.
32 R. Wahab, S. G. Ansari, Y. S. Kim, H. K. Seo, G. S. Kim, G. Khang and H. S. Shin, *Mater. Res. Bull.*, 2007, **42**(9), 1640–1648.
33 R. Wahab, S. G. Ansari, Y. S. Kim, H. K. Seo and H. S. Shin, *Appl. Surf. Sci.*, 2007, **253**, 7622–7626.
34 R. Wahab, S. G. Ansari, Y. S. Kim, G. Khang and H. S. Shin, *Appl. Surf. Sci.*, 2008, **254**(7), 2037–2042.
35 R. Wahab, Y. S. Kim, I. H. Hwang and H. S. Shin, *Synth. Met.*, 2009, **159**, 2443–2452.
36 X. Jin, M. Götz, S. Wille, Y. K. Mishra, R. Adelung and C. Zollfrank, *Adv. Mater.*, 2013, **25**(9), 1342–1347.
37 W. Li, D. S. Mao, Z. H. Zheng, X. Wang, X. H. Liu, S. C. Zhu, Q. Li and J. F. Xu, *Surf. Coat. Technol.*, 2000, **128**, 346–350.
38 S. A. Studenikin, N. Golego and M. Cocivera, *J. Appl. Phys.*, 1998, **84**(4), 2287–2294.
39 B. Liu and H. C. Zeng, *J. Am. Chem. Soc.*, 2003, **125**(15), 4430–4431.
40 H. J. Egelhaaf and D. Oelkrug, *J. Cryst. Growth*, 1996, **161**, 190–194.
41 S. K. Pardeshi and A. B. Patil, *J. Mol. Catal. A: Chem.*, 2009, **308**, 32–40.
42 J. L. Bresloff and D. M. Crothers, *Biochemistry*, 1981, **20**(12), 3547–3553.

43 S. Ostrovsky, G. Kazimirsky, A. Gedanken and C. Brodie, *Nano Res.*, 2009, **2**(11), 882–890.
44 T. Mosmann, *J. Immunol. Methods*, 1983, **65**, 55–63.
45 E. Chang, N. Thekkek, W. W. Yu, V. L. Colvin and R. Drezek, *Small*, 2006, **12**, 1412–1417.
46 R. R. Letfullin, C. B. Iversen and T. F. George, *Nanomedicine*, 2011, **7**(2), 137–145.
47 M. Ahamed, M. J. Akhtar, M. A. Siddiqui, J. Ahmad, J. Musarrat, A. A. Al-Khedhairy, M. S. Al-Salhi and S. A. Alroka yan, *Toxicology*, 2011, **283**, 101–108.
48 R. Wahab, Y. B. Yang, A. Umar, S. Singh, I. H. Hwang, H. S. Shin and Y. S. Kim, *J. Biomed. Nanotechnol.*, 2012, **8**, 424–431.
49 R. Wahab, S. Dwivedi, A. Umar, S. Singh, I. H. Hwang, H. S. Shin, J. Musarrat, A. A. Al-Khedhairy and Y. S. Kim, *J. Biomed. Nanotechnol.*, 2013, **9**, 441–449.
50 R. Wahab, S. Dwivedi, F. Khan, Y. K. Mishra, I. H. Hwang, H. S. Shin, J. Musarrat and A. A. Al-Khedhairy, *Colloids Surf., B*, 2014, **123**, 664–672.
51 T. Amna, H. V. Ba, M. Vaseem, M. S. Hassan, M. S. Khil, Y. B. Hahn, H. K. Lee and I. H. Hwang, *Appl. Microbiol. Biotechnol.*, 2013, **97**(12), 5545–5553.
52 S. J. Soenen, B. Manshian, J. M. Montenegro, F. Amin, B. Meermann, T. Thiron, M. Cornelissen, F. Vanhaecke, S. Doak, W. J. Parak, S. D. Smedt and K. Braeckmans, *ACS Nano*, 2012, **6**(7), 5767–5783.
53 A. M. Alkilany and C. J. Murphy, *J. Nanopart. Res.*, 2010, **12**(7), 2313–2333.
54 R. U. Jänicke, P. Ng, M. L. Sprengart and A. G. Porter, *J. Biol. Chem.*, 1998, **273**(25), 15540–15545.
55 J. C. Timmer and G. S. Salvesen, *Cell Death Differ.*, 2007, **14**, 66–72.
56 W. C. Earnshaw, L. M. Martins and S. H. Kaufmann, *Annu. Rev. Biochem.*, 1999, **68**, 383–424.
57 L. K. Limbach, Y. Li, R. N. Grass, T. J. Brunner, M. A. Hinter mann, M. Muller, D. Gunther and W. J. Stark, *Environ. Sci. Technol.*, 2005, **39**(23), 9370–9376.
58 S. M. Hussain and J. J. Schlager, *Oxf. J.*, 2009, **108**, 223–224.